Journal of
Nanoscience and Nanotechnology
Vol. 9, 3193–3200, 2009

The Effects of the Modulated Magnetic Fields on Electronic Structures of Graphene Nanoribbons

J. Y. Wu[1,*], Y. H. Chiu[2], J. Y. Lien[1], and M. F. Lin[1,*]

[1] Department of Physics, National Cheng Kung University, Tainan, Taiwan 701
[2] Institute of Physics, National Chiao Tung University, 300 Hsinchu, Taiwan

The low-energy magnetoelectronic structures of nanographene ribbons under a modulated magnetic field are investigated by the Peierls tight-binding model. They are dominated by the field strength, period, phase, the ribbon width, and edge structure. The modulated magnetic field could add state degeneracy, modify energy dispersions, alter subband spacings, affect carrier-density distributions, create additional band-edge states, and cause semiconductor-metal transitions. The main features of energy bands are directly reflected in density of states, such as the position, height, structure, and number of the prominent peaks. These results immensely differ from those in a uniform magnetic field. Significant differences between a 1D graphene ribbon and a 2D electron gas are also found.

Keywords: Nanographene Ribbon, A Modulated Magnetic Field.

1. INTRODUCTION

The honeycomb lattices of carbon atoms known as graphene, was isolated and found stable, highly crystalline, and chemically inert at ambient conditions.[1,2] The half-integer QHE and massless Dirac electronic behavior[3–5] have been investigated recently. The one-dimension (1D) ribbons, the layered graphene with nanometer sized widths, can be realized by using the mechanical method[6] and the lithographically patterned method.[7,8] The essentially physical properties of graphene nanoribbons are dominated by the geometry structures (width and edge structure). The 1D carbon-related material has motivated many works in recent years, such as band structure,[9–11] optical absorption spectra,[12,13] transport properties,[8,14–18] deformation effect,[19] and coulomb excitations.[20] There are two basic types of nanographene ribbons according to edge structure.[21] The zigzag ribbons have special partial flat bans at low energy.[22] Such electronic states are the edge states that localize at the outmost zigzag positions. The armchair ribbons, which are oriented perpendicular to the zigzag ribbon, have an oscillatory energy-gap dependence on ribbon width.[10,11]

Nanographene ribbons under uniform electric[12,14] and magnetic fields[9,23] have been calculated theoretically. The former would shift the Fermi level, modify the energy dispersions, alter the subband spacing, produce the new edge state, change the band gap, and cause semiconductor-metal transitions. Especially for zigzag ribbons, the degeneracy of partial flat bands at the Fermi level is lifted by the electric field, but the electronic states are still localized at zigzag edge. The perpendicular uniform magnetic field has different influences on the low-energy electronic structures. The dispersionless Landau levels develop while the ribbon width is wide enough, otherwise the partial flat bands are formed. There exist current-caring states at or close to the interface with the ribbon edge at any case. These strong field effects can lead to interesting physical phenomena, and they can be utilized in carbon-based electronic devices as well.

In this paper, a spatially modulated magnetic field is applied to the nanographene ribbon. Its strength varies along the transverse direction of the ribbon. Much research has been dealt with energy bands[24–26] and magnetoconductances[27–33] for a two-dimensional electron gas (2DEG) under nonuniform magnetic fields, and also for graphene recently.[34] However, crystal structure and quantum confinement of 1D ribbons cause some distinct electronic properties compared with a 2DEG in such a field, such as Landau level energies, isotropic properties, state degeneracy. The dependence of magnetoelectric properties on the field strength, period, phase, the ribbon width, and edge structure will be investigated in detail.

2. THEORY

The two typical topological shapes, armchair and zigzag, are depicted in Figure 1. The structure consists of

*Authors to whom correspondence should be addressed.

 1533-4880/2009/9/3193/008 doi:10.1166/jnn.2009.042

RESEARCH ARTICLE

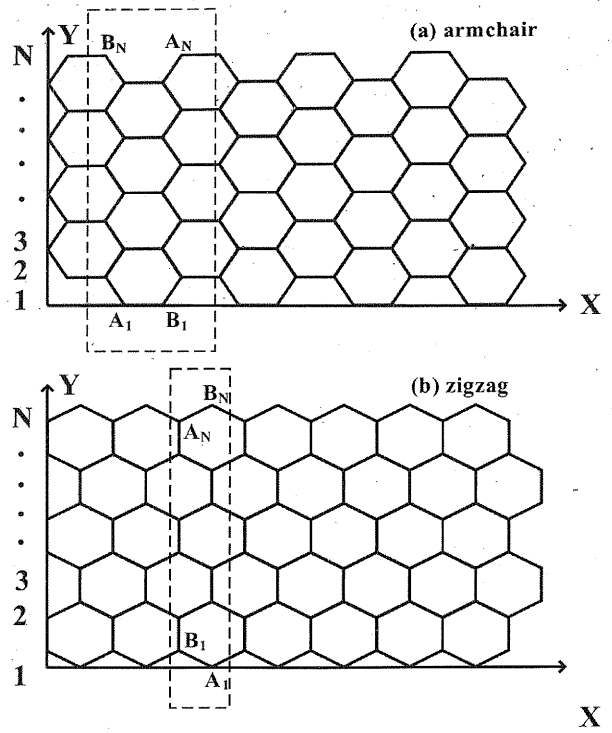

Fig. 1. Nanographene ribbons with (a) armchair edge and (b) zigzag edge.

sublattices A and B, and the C–C bond length is $b = 1.42$ Å. The ribbon width W is directly proportional to N, the number of dimer lines or zigzag lines. The periodical length along the x-axis is $3b$ ($\sqrt{3}b$) for an armchair (a zigzag) ribbon. The unit cell contains N A-type atoms and N B-type atoms. Each carbon atom is connected by strong σ bonds between sp^2 hybridized orbitals of $2s$, $2p_x$, and $2p_y$, performing a framework of honeycomb lattice, while two $2p_z$ orbitals form relatively weak bonds called π bonds. Hence, it is a good approximation to calculate π electrons alone to investigate the low-energy electronic structures.

The $2p_z$ wave function is the linear superposition of the $2N$ tight-binding functions. Graphene ribbons are assumed to be subject to a spatially modulated magnetic field $\mathbf{B} = B' \sin Ky\hat{z}$ perpendicular to the graphene plane. The modulation period length along the y-axis is $2\pi/K = \lambda$, where λ is in unit of ribbon width W. The Peierls phase is characterized by the vector potential in the form, $\mathbf{A} = B'/K \cos Ky\hat{x}$. The nearest-neighbor hopping integral associated with the extra position-dependent phase is

$$\langle b_{j\mathbf{k}}|H_{\mathbf{B}}|a_{i\mathbf{k}}\rangle = \gamma_0 \exp\left\{i\left[\mathbf{k}\cdot(\mathbf{R}_i - \mathbf{R}_j) + \frac{2\pi}{\Phi_0}\int_{\mathbf{R}_i}^{\mathbf{R}_j}\mathbf{A}\cdot d\mathbf{r}\right]\right\} \quad (1)$$

where $\gamma_0 = 2.5$ eV Ref. [35] is the value of π-bond hopping amplitude at zero fields. The magnetic modulation period induces the periodical boundary condition along the y-axis so that the corresponding Peierls phase is related to the y-coordinate of atoms. The first Brillouin zone is defined by $\pi/I_x \geq k_x \geq -\pi/I_x$, where $I_x = 3b$ ($\sqrt{3}b$) for an armchair (a zigzag) ribbon. As a result, the Hamiltonian matrix is a $2N \times 2N$ Hermitian matrix. For an armchair ribbon, it could be expressed as

$$H_{lm} = \begin{cases} -\gamma_0 e^{i\theta_1} e^{-ik_x b} & \text{if } l = 2i-1;\ m = 2i \\ -\gamma_0 e^{i\theta_2} e^{-ik_x b/2} & \text{if } l = m-1;\ m = 2i-1 \\ -\gamma_0 e^{i\theta_3} e^{ik_x b/2} & \text{if } l = m-3;\ m = 2i \\ 0 & \text{others} \end{cases} \quad (2)$$

$\theta_1 = (\lambda\Phi'/3)(N-1)\cos[4\pi n/\lambda(N-1)]$; $\theta_2 = \theta_3 = (\lambda^2\Phi'/6\pi)(N-1)^2\cos[\pi(4n-1)/\lambda(N-1)]\sin[\pi/\lambda(N-1)]$. The magnetic flux $\Phi' = 3\sqrt{3}B'b^2/2\Phi_0$ (in unit of a flux quantum $\Phi_0 = hc/e = 4.1356 \times 10^{-15}$ $\mathrm{T \cdot m^{-2}}$) is the flux through a hexagon by the B' field.

As to a zigzag ribbon, the Hamiltonian matrix is given by

$$H_{lm} = \begin{cases} 2\gamma_0 \cos(k_x a/2 - \theta) & \\ \qquad \text{if } l = 2i-1;\ m = 2i & \\ -\gamma_0 \quad \text{if } l = m-1;\ m = 2i-1 & \\ 0 \qquad \text{others} & \end{cases} \quad (3)$$

$\theta = -\lambda^2(\Phi'/3\pi)(3N/2-1)^2\cos[\pi(12n-1)/(3N-2)]\sin[\pi/(3N-2)]$. By diagonalizing the Hamiltonian matrix, state energy $E^{c,v}$ and wave function $\Psi^{c,v}$ are derived. The superscript $c(v)$ represents the unoccupied conduction band (the occupied valence band).

3. MAGNETOELECTRONIC PROPERTIES

According to the tight-binding model[35] calculation, armchair ribbons of $N \neq 3I+2$ (I an integer) are direct-gap semiconductors, and those of $N = 3I+2$ are metals. The existence of partial flat bands leads all zigzag ribbons to gapless systems. The armchair ribbons of $N = 600$ and 599 as well as zigzag ribbons of $N = 350$ are chosen for typical researches. The low energy electronic structure of $N = 600$ armchair ribbon in the absence of magnetic field, is shown in Figure 2(a). The occupied π states $E^v(\gamma_0)$ are symmetric to the unoccupied π^* states $E^c(\gamma_0)$ with respect to $E_F = 0$, even under the modulated magnetic field. Only the latter are discussed in this work. The energy bands are all non-degenerate parabolic dispersive with band-edge states at $k_x = 0$, and exhibit a band gap found $0.003\gamma_0$ ($\approx$0.0075 eV) near E_F. The neighboring energy spacings become smaller as k_x grows. The band curvatures gradually approximate to zero with the decrease in energy.

The modulated magnetic field greatly influences the energy dispersion of armchair ribbons in many aspects: it would modify band curvatures or effective masses, create extra band-edge states, enhance state degeneracy, alter

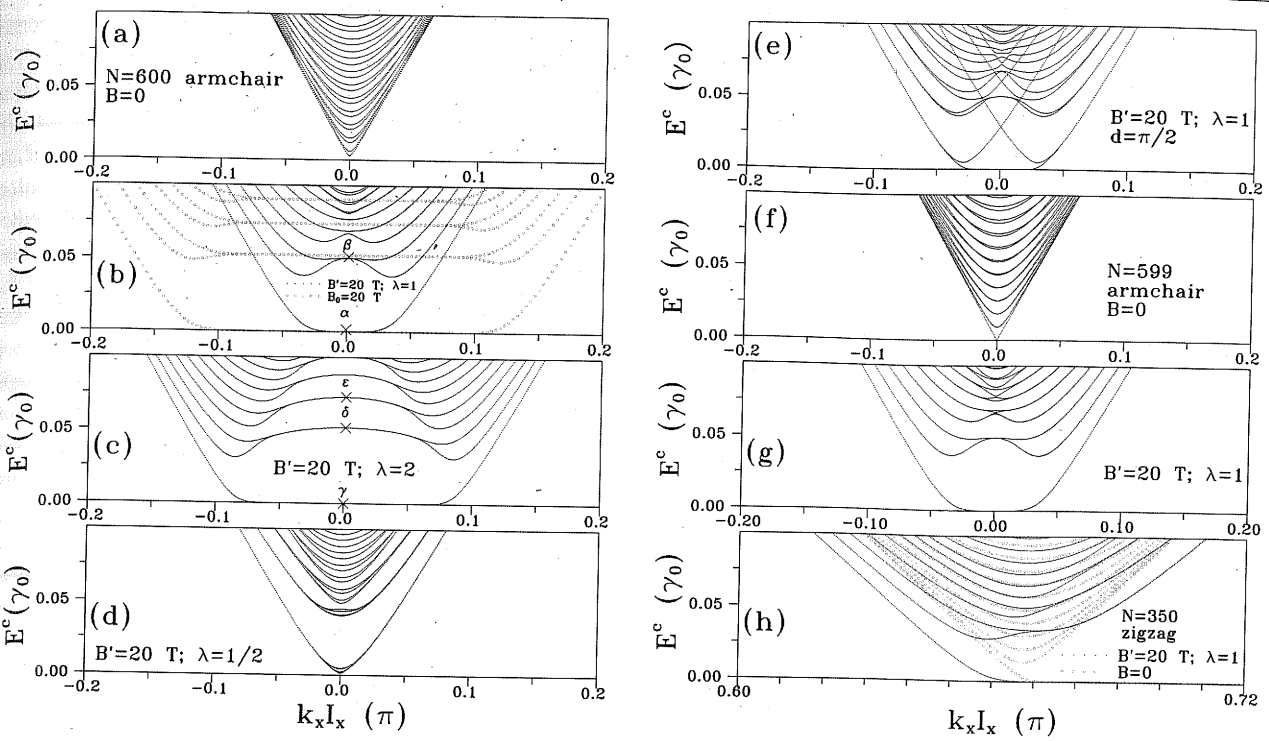

Fig. 2. The low π-electronic structures of the $N = 600$ armchair ribbon without B (a), under the modulated magnetic field $B' = 20$ T at different period λ: (b) $\lambda = 1$, (c) $\lambda = 2$, and (d) $\lambda = 1/2$. With different field phase, ribbon width and edge structure: (e) $B' = 20$ T; $\lambda = 1$; $d = \pi/2$, (f) the $N = 599$ armchair ribbon at $B' = 20$ T; $\lambda = 1$. The $N = 350$ zigzag ribbon at $B' = 20$ T; $\lambda = 1$ at (g) $-0.72\pi \le k_x I_x \le -0.6\pi$, and (h) $0.6\pi \le k_x I_x \le 0.72\pi$. Also shown in (b) is $B_0 = 20$ T. Zigzag ribbon without B is shown in (g) and (h) for comparison.

subband spacings, and change energy gap. In Figure 2(b), the $N = 600$ armchair ribbon at field strength $B' = 20$ T and period $\lambda = 1$ is displayed (solid circles). The 1D subbands exhibit oscillating parabolic and parabolic dispersions. The former create two extra band-edge states, which locate respectively at the left- and right-hand sides of the original one, while the latter retain their band-edge states at $k_x = 0$. The number of energy bands is appreciably reduced because each energy band becomes doubly degenerate at low energy, and the subband spacings are enhanced. At $E = 0.05\gamma_0$, two oscillating parabolic subbands merge together, which brings about four-fold state degeneracy near $k_x = 0$ and weak energy dispersion around it. For positive k_x and negative k_x respectively, the four-fold degenerate states are divided into two. The energy gap approaches to zero, as two partial flat bands congregate at the Fermi level; that is quasi-Landau level. As the field strength grows up, more drastically oscillating subbands, larger subband spacings, smaller band curvatures, and longer partial flat bands are derived.

The $N = 600$ armchair ribbon in a uniform magnetic field is also plotted for comparison [open circles in Fig. 2(b)]. It exhibits the composite bands, made up of the partial flat bands and the parabolic bands, with the former constituent bands being doubly degenerate due to the hexagonal networks of graphene ribbons and the latter being non-degenerate. In a classical description, electrons under a uniform magnetic field, move along an circular equipotential line, and become dispersionless Landau levels, except those near the ribbon edge (corresponding to parabolic like dispersions at large k_x's). The ribbon edge could be represented as a confining potential;[5] therefore, the electron energy is raised and moves along the edge. The wavenumber range of partial flat bands is dominated by the field strength and ribbon width, but their spacings depend only on field strength. Moreover, the band-edge states no longer locate at $k_x = 0$, but at the two extremities of partial flat bands. Also a semiconductor-metal transition is derived. However, the energy bands display some notable distinctions compared with those in a modulated magnetic field, such as the wavenumber range of partial flat bands, subband curvatures, state degeneracy, band-edge-state positions and energies. This is mainly resulting from the fact that a modulated magnetic field induces the space-dependent (k_x-dependent) potential, and that the fully closed cyclotron orbit of an electron is no longer a circle, but a spiral-like.[24, 36] In this way, the k_x states hardly flock together, and oscillating parabolic subbands appear.

The modulation period λ plays an important role in electronic structures. As λ is doubled [Fig. 2(c)], the average magnetic field $|B|$ is no longer zero, and it reaches its maximum at the ribbon center and minimum at the two edges. Generally speaking, the energy bands under such a field become more similar to those under a uniform magnetic field, e.g., the state degeneracy, the width of partial flat

bands, and band curvatures. The subbands are all oscillating parabolic bands and they are coupled with a band-edge state at $k_x = 0$, which is doubly degenerate and has weak energy dispersion. In the smaller or larger k_x region, these degenerate states are separated with the creation of four extra band-edge states, whose positions gradually approach $k_x = 0$ as the increase in energy. With a comparison to the band structures at $\lambda = 1$, the longer partial flat bands, more oscillating parabolic subbands, and lower band curvatures are observed. This means that the field with larger period length would have better ability in flocking the electrons. Also the band-edge state positions and their energies are changed. On the contrary, as the field period is reduced to $\lambda = 1/2$ [Fig. 2(d)], no electronic states flock together, and the energy bands are almost identical to the $B = 0$ condition. Most of them exhibit parabolic dispersions, and a band gap exists near the Fermi level. Around $k_x = 0$, all electronic states are non-degenerate, except that the lowest ones are doubly degenerate. However, at large k_x, the state degeneracy becomes four-fold, which is twice (quadruply) as much as that at $\lambda = 1$ ($\lambda = 2$). This result directly indicates that the state degeneracy depends on the node number of the modulated magnetic field. A brief summary can be given: the energy bands under a more slowly modulated field (with larger λ) would present features which more resemble those under a uniform magnetic field. The reason is that the electrons experience a smaller field gradient ∇B (Refs. [24, 36]) and, thus, have a correspondently smaller drift velocity. Consequently, the wider k_x range of quasi-Landau-levels is obtained.

The wave-function distributions deserve a further investigation. The squared amplitude, $|\Psi|^2$, of $\alpha - \epsilon$ points [noted in Figs. 2(b–c)] are drawn in Figure 3. They present oscillatory behavior. The α point is where the quasi-Landau-levels appear at $\lambda = 1$. It is contributed by those electrons localized around the $N = 125$ and 475 dimer lines on the ribbon width, where the magnetic field approaches its maximum. When the wave number deviates from $k_x = 0$, the carrier-density distribution is pushed into ribbon edge ($N = 1$ and 600) or center ($N = 300$), and the energy band becomes dispersive. The β point is the central-band-edge state of the lowest oscillatory subband. It displays two extra local minima near the two maximal-magnetic-field regions respectively, and the localization becomes weaker. Similarly, for $\lambda = 2$, the electrons at the γ-point state concentrate on the ribbon center, which is the maximal-magnetic-field point in this case. The δ and ε points are the lowest two central-band-edge states, and they have one and two local minima around the ribbon center, respectively. As to $\lambda = 1/2$ condition, the carrier-density distribution at $k_x = 0$ becomes delocalized, because the insufficient field period length makes the electrons could not be constrained at each maximal-magnetic-field point independently. In this way, the quasi-Landau-levels could not appear.

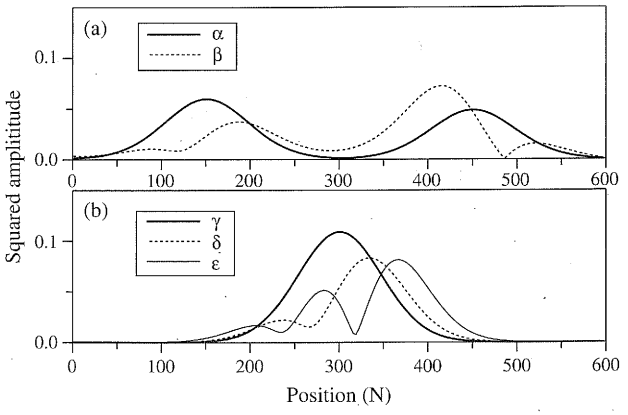

Fig. 3. The position-dependent carrier density along the $\hat{y}$ direction for (a) the α and β states (Fig. 2(b)); (b) the γ, δ, and ε states (Fig. 2(c)).

The finite width of ribbon systems causes the modulation-field phase to be critical for low-energy magnetoelectronic properties. In Figure 2(e), the modulated magnetic field is transformed from $\mathbf{B} = B' \sin Ky\hat{z}$ to $\mathbf{B} = B' \cos Ky\hat{z}$. Such a field has the maxima at two ribbon edges and center. The metal-semiconductor transition still occurs with two non-degenerate partial flat bands congregating at the Fermi level. The oscillating parabolic subbands are to exhibit composite degeneracy at low energy, the single and double degeneracy. However they become non-degenerate at high energy. Especially, there exist four parabolic bands with band-edge states at $k_x \neq 0$ between the oscillating subbands, two of them intersecting at $E = 0.025\gamma_0$ and the other two at $E = 0.05\gamma_0$. The electronic states on these dispersions are localized at ribbon edges. The fewer degenerate states and stronger dispersions in energy band reveal that the ribbon edges would substantially hinder the electrons from flocking together in such a field.

Different ribbon widths and edge shapes under the modulated magnetic field are also discussed. At $B = 0$, the $N = 599$ metallic armchair ribbon exhibits the linear bands and the 1D parabolic bands [Fig. 2(f)]. The linear bands cross each other at E_F and thus the $N = 599$ ribbon is a metal. Due to the size effect, the state energies of 1D parabolic bands are quite different from those of the $N = 600$ ribbon, as shown in Figure 2(a). A modulated magnetic field would curve the linear bands into parabolic bands, and produce degenerate partial flat bands at E_F as the field strength rises up to $B' = 20$ T [Fig. 2(g)]. As $E > 0.05\gamma_0$, state energies and degeneracy of band-edge states at $k_x = 0$ are different from those of the $N = 600$ armchair. This discrepancy results from the wave function touching two ribbon edges, and thus these states depend on the ribbon width.[23] In contrast, the state energies at large k_x remain the same in the two systems, because the electronic distributions are confined at ribbon edges or the zero-magnetic-field region, and are independent of ribbon width. Moreover, the energy bands of the

two systems are identical below $E = 0.05\gamma_0$. That is, the electron energies are only dominated by the field strength as the quasi-Landau levels are formed or the wavefunction distributions become localized.

The edge structure of ribbon also plays a major part in electronic properties. The low energy dispersion of $N = 350$ zigzag is shown in Figure 2(h). At $B = 0$ (open circles), it exhibits parabolic subbands and partial flat bands at $E_F = 0$. The former have band-edge states at $k_x I_x = 2\pi/3$. The latter are distributed in the range of $2\pi/3 \leq k_x I_x \leq \pi$ and belong to the edge states,[22] which have been demonstrated by STM and STS.[37–39] The wavenumber range of partial flat bands would be stretched by a modulated magnetic field (solid circles). The extended part is generated by electrons located at maximal-magnetic-field regions, and dominated by the field strength and period. Accordingly, the larger B' and larger λ would cause the longer partial flat bands. Moreover, the low energy subband curvatures, spacings, degeneracy, the band-edge-state positions and energies are also modified.

The correspondence between the energy gap and the modulated magnetic field is shown in Figure 4. For the $N = 600$ semiconducting armchair ribbon, its band gap is determined by the $k_x = 0$ state of the parabolic band in Figure 2(a). Band gap is reduced by B' first, and as B' further increases, it disappears. At the same time, the parabolic bands are transformed into partial flat bands (quasi-Landau levels), and the metal-semiconductor transition is derived. The more slowly the magnetic field varies (at larger λ), the more easily the quasi-Landau level can be induced, and the smaller magnetic field is needed to derive the transition. On the other hand, an appropriate phase shift d could also facilitate the transition. As to the $N = 599$ metallic armchair ribbon, a very weak magnetic field could convert the linear bands at the Fermi level into parabolic bands, and a direct energy gap is observed. E_g augments with the increasing B' initially until it reaches a maximal value, and then begins to drop. The relation between this maximal value and λ presents an oscillatory dispersion. When the B' is large enough, the quasi-Landau level appears, and the band gap approaches to zero.

The energy gaps have a close relation to the ribbon width, shown in Figure 4(c). They are grouped into two families, $N \neq 3I+2$ and $N = 3I+2$. The band gaps of the $N = 3I+1$ ribbons at $B' = 10$ T and $\lambda = 1$ are the largest. With the increase in ribbon width, the band gaps decay very fast, and become too small to be differentiated as $N > 750$. Doubling the field period or strength would also diminish the band gap substantially. Under the former condition the band gaps would be hardly observable. Experimentally, the larger field periods and the wider ribbon widths are easier to be realized, and therefore, the metal-semiconductor transition could be perceived at small field strength.

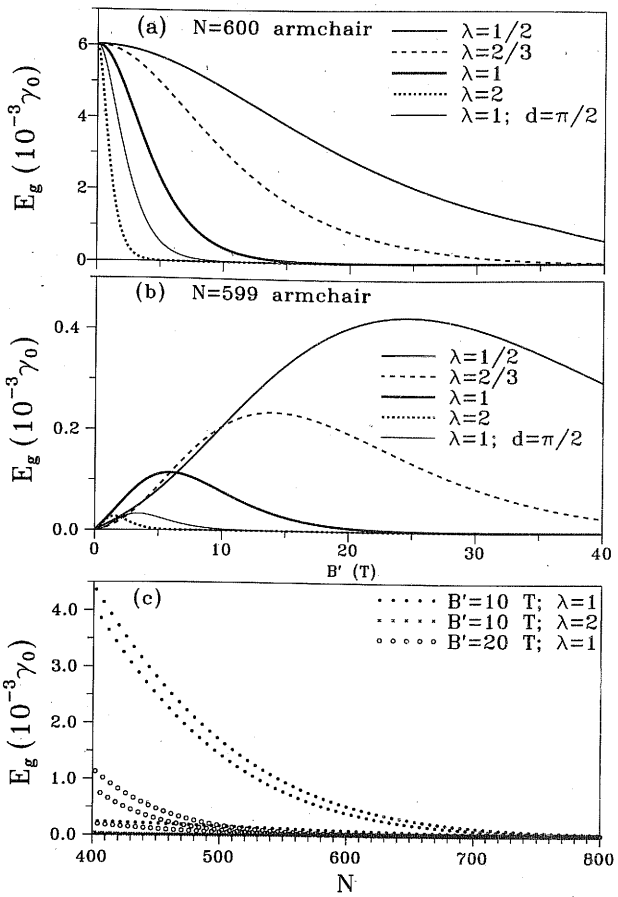

Fig. 4. The magnetic-strength-dependent energy gaps are calculated for the (a) $N = 600$ and (b) $N = 599$ armchair ribbons at different λ and d's. The width-dependent energy gaps at different B' and λ's are plotted in (c).

Density of states (DOS), which reveals the main features of energy bands, is defined as

$$D(\omega) = \frac{2I_x}{2N}\int_{1\text{stBZ}} \frac{dk_x}{2\pi} \frac{\Gamma}{\pi[(E(k_x)-\omega)^2+\Gamma^2]} \quad (4)$$

$\Gamma(=0.0001\gamma_0)$ is the phenomenological broadening parameter. The light curves in Figures 5(a), (e) and (f), respectively, present the low frequency DOS for $N = 600$, 599 armchair and $N = 350$ zigzag ribbons in the absence of the magnetic field. Each of them demonstrates considerable asymmetric square-root divergences at $\omega \neq 0$. These peaks derived from the critical points (band-edge states) of 1D concave-upward parabolic bands. Different ribbon widths and edge structures would exhibit distinct features at the Fermi level in DOS. The armchair ribbon has zero DOS for semiconductor [Fig. 5(a)], and a plateau for metal [Fig. 5(e)]. The former and the latter are respectively determined by the band-edge states of the 1D parabolic dispersions [Fig. 2(a)] and linear bands [Fig. 2(f)] at $E_F = 0$. For the zigzag ribbon [Fig. 5(f)], a delta-function-like peak is shown at $\omega = 0$, owing to the edge states of partial flat bands.

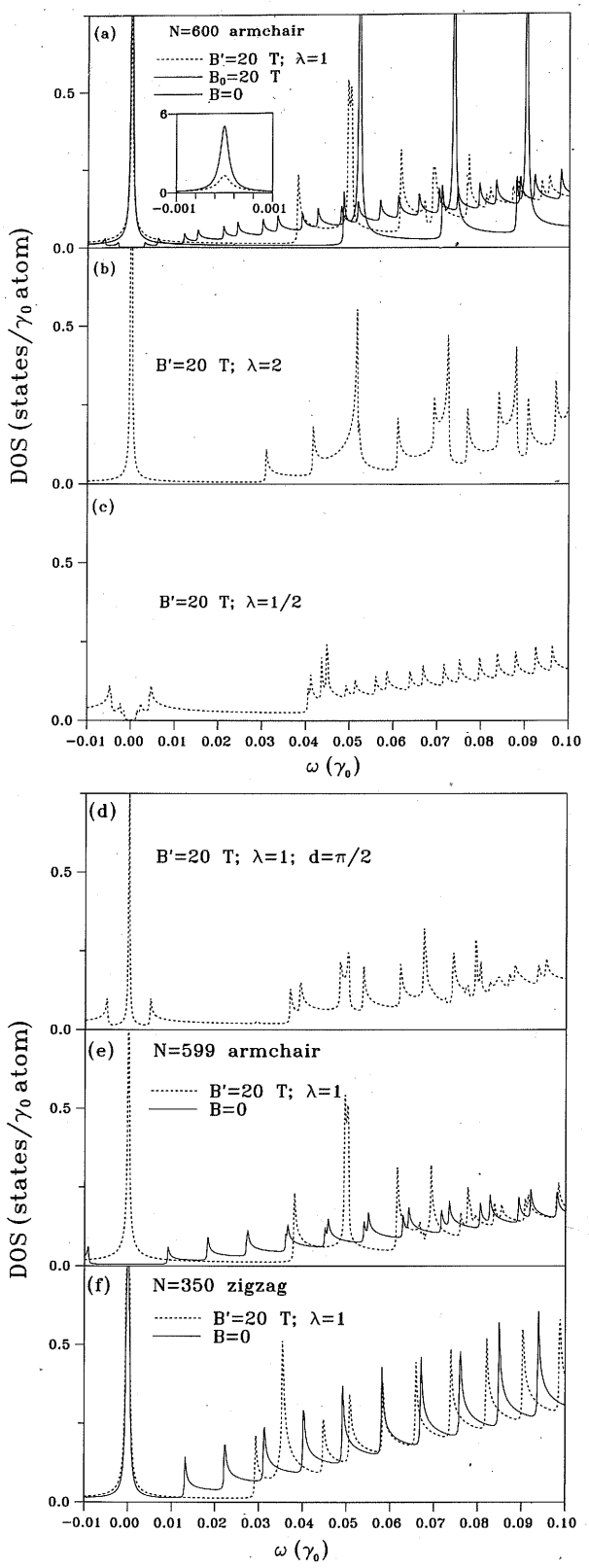

Fig. 5. Density of states for the $N = 600$ armchair ribbon at (a) $B' = 20$ T; $\lambda = 1$, and $B_0 = 20$ T, (b) $B' = 20$ T; $\lambda = 2$, (c) $B' = 20$ T; $\lambda = 1/2$, and (d) $B' = 20$ T; $\lambda = 1$; $d = \pi/2$. Those for (e) the $N = 599$ armchair ribbon at $B' = 20$ T; $\lambda = 1$, and (f) the $N = 350$ zigzag ribbon at $B' = 20$ T; $\lambda = 1$. Those without B are also shown in (a), (e) and (f) for comparison. The inset of (a) presents DOS near $\omega = 0$.

A modulated magnetic field has conspicuous effects on the divergent forms, the number, the heights, and the positions of the prominent peaks in DOS. For the $N = 600$ armchair ribbon at $B' = 20$ T and $\lambda = 1$ [Fig. 5(a)], the band gap closes as a symmetric delta-function-like peak emerges at the Fermi level, which arises from the quasi-Landau Levels. Because of the augmentation in subband degeneracy, the number peaks is evidently reduced while their heights increase. A pair of asymmetric sharp peaks are located around $\omega = 0.05\gamma_0$. Such divergences are caused by band-edge states of 1D oscillating parabolic bands. The increasing field strength could enhance the oscillating parabolic subbands, lower the band curvatures, and add degenerate states. Consequently, it would broaden the peak spacings, induce more high peaks, and decrease the number of peaks. Furthermore, that a uniform magnetic field has better ability in grouping electronic states could be also demonstrated in DOS [solid line in Fig. 5(a)]. Several strong delta-function-like peaks exist at $\omega \neq 0$ with each one accompanying another asymmetric square-root divergent peak. The former is the result of the partial flat subbands (Landau levels), and the latter is dominated by the extra band-edge states at the two extremities of them.

Raising the field period λ to 2, those paired oscillating parabolic bands [in Fig. 2(c)] with four band-edge states at $k_x \neq 0$ and one at $k_x = 0$, would induce a great deal of strong squared-root divergences, which are performed by $D(\omega) \sim 1/\sqrt{\omega - \omega_0}$ and $D(\omega) \sim 1/\sqrt{\omega_0 - \omega}$, respectively. The latter are the higher ones located at $\omega = 0.05$, 0.07, and $0.09\gamma_0$. Such frequencies are very close to where Landau-levels appear in Figure 5(a). Furthermore, the first asymmetric-peak frequency lowers compared with that at $\lambda = 1$. However, reducing the period length would decrease the field's ability in flocking electrons [as seen Fig. 2(d)], and it leads to the results that only the first several peaks are conspicuously influenced in Figure 5(c), that no sharp peak is observed, and that a band gap arises near $\omega = 0$.

The different field phases, ribbon widths, and edge shapes, are the other three important elements in DOS [Figs. 5(d–f)]. At $B = B' \cos Kx$ [Fig. 5(d)], the DOS exhibits no sharp peak except the delta-function-like peak at $\omega = 0$. The additional parabolic bands in Figure 2(e) lead to more extended states, and the lowest band-edge states of them produce the first asymmetric peak in the vicinity of $\omega = 0$. This low frequency peak near the Fermi energy would be important for transport properties. The DOS of $N = 599$ armchair ribbon is shown in Figure 5(e). The low-energy plateau comes from the linear bands near E_F [Fig. 2(f)] and would be transformed to a sharp peak (partial flat bands induce) by a modulated magnetic field. The first few peaks are almost identical to those of the $N = 600$ armchair, and they depend only on the field strength. At $\omega > 0.06\gamma_0$, the two width ribbons differ from each other in peak number, heights, and frequencies. For $N = 350$ zigzag ribbon in the same field, the main feature

of DOS does not change except for the peaks near $\omega = 0$. The delta-function-like peak at the Fermi level would be evidently heightened at larger B' or larger λ. The magneto electronic density of states discussed above could be experimentally verified by scanning tunneling spectroscopy (STS),[40–42] resonant Raman scattering,[43–45] and optical absorption and emission measurement.[46–49]

The transformation from 2DEG to 1D superlattices via the application of a spatially modulated magnetic field has been extensively studied.[24–33] Their electronic properties can be clearly described by the shape of the effective potential. This method is also used to explain the low energy spectra for narrow-gap semiconductors.[50] A 1D graphene ribbon also displays analogic characteristic of band structures, such as the composite behavior in state degeneracy, the extra band-edge states, and the change of band curvatures. However, some differences are observed between a 2DEG and a 1D ribbon. A 2DEG exhibits no partial flat bands at zero energy, and the magnetoelectronic structure is independent of the modulation direction. It is the hexagonal structure of carbon systems that results in such differences. Moreover, state degeneracy is independent of modulation period. Without net magnetic field, i.e., $\langle B \rangle = 0$, the absence of Hall resistance is expected; however, this is not true when the ribbon width is narrower than field period length ($\lambda > 1$), and therefore $\sigma_{xy} \neq 0$. The above-mentioned differences are due to the quantum confinements of a 1D ribbon.

4. CONCLUSION

In this paper, we have studied the effects of the modulated magnetic field on the low-energy electronic structures of nanographene ribbons within the tight-binding approximation. Energy bands and density of states are mainly determined by the field strength, period, phase, the ribbon width, and edge shape. The modulated magnetic fields modify energy dispersions, create extra band-edge states, alter subband spacings, affect wave function, add state degeneracy, and induce semiconductor-metal transitions. There are partial flat bands at the Fermi level and oscillating parabolic subbands with extra band-edge states. These results indicate that, in the presence of a modulated magnetic field, transport properties are one dimension. The distribution of wave function becomes localized, which is dominated by the magnetic field. The state degeneracy is related to the node number of the modulated magnetic field, but is independent of the field strength. The metal-semiconductor transitions are easily to be achieved, and they strongly depend on the fields and the ribbon widths. The partial flat bands at $E_F = 0$ in zigzag ribbons could survive any modulated magnetic field, while the range of wave vector k_x could be extended. The hexagonal symmetry and the quantum confinements cause a 1D ribbon to differ from a 2DEG. The differences are the existence of the partial flat bands at zero energy, dependence on the modulation direction, state degeneracy. Density of states responds directly to the above-mentioned features of energy bands, such as the divergent structures, the heights, the frequencies, and the number of peaks. It exhibits strong square-root divergences corresponding to the band-edge states in 1D parabolic bands. Also the partial flat bands induce delta-function-like divergences at the Fermi level. The predicted electronic properties are associated with transport properties and magneto-optical spectra. These effects that can be measured by experiments would demonstrate the influence of a magnetic modulation on nanographene ribbons.

References and Notes

1. Y. Zhang, Y.-W. Tan, H. L. Stormer, and P. Kim, *Nature (London)* 438, 201 (**2005**).
2. S. Stankovich, D. A. Dikin, G. H. B. Dommett, K. M. Kohlhaas, E. J. Zimney, E. A. Stach, R. D. Piner, S. T. Nguyen, and R. S. Ruoff, *Nature (London)* 442, 282 (**2006**).
3. K. S. Novoselov, A. K. Geim, S. V. Morozov, D. Jiang, M. I. Katsnelson, I. V. Grigorieva, S. V. Dubonos, and A. A. Firsov, *Nature* 438, 197 (**2005**).
4. A. De Martino, L. Dell'Anna, and R. Egger, *Phys. Rev. Lett.* 98, 066802 (**2007**).
5. N. M. R. Peres, A. H. Castro Neto, and F. Guinea, *Phys. Rev. B* 73, 241403 (**2006**).
6. H. Hiura, *Appl. Surf. Sci.* 222, 374 (**2004**).
7. C. Berger, Z. Song, X. Li, X. Wu, N. Brown, C. Naud, D. Mayou, T. Li, J. Hass, A. N. Marchenkov, E. H. Conrad, P. N. First, and W. A. de Heer, *Science* 3012, 1191 (**2006**).
8. M. Y. Han, B. Özyilmaz, Y. Zhang, and P. Kim, *Phys. Rev. Lett.* 98, 206805 (**2007**).
9. K. Wakabayashi, M. Fujita, H. Ajiki, and M. Sigrist, *Phys. Rev. B* 59, 12 (**1999**).
10. M. Ezawa, *Phys. Rev. B* 73, 045432 (**2006**).
11. H. Zheng, Z. F. Wang, T. Luo, Q. W. Shi, and J. Chen, *Phys. Rev. B* 75, 165414 (**2007**).
12. C. P. Chang, Y. C. Huang, C. L. Lu, J. H. Ho, T. S. Li, and M. F. Lin, *Carbon* 44, 508 (**2006**).
13. H. Hsu and L. E. Reichl, *Phys. Rev. B* 76, 045418 (**2007**).
14. D. S. Novikov, *Phys. Rev. Lett.* 99, 056802 (**2007**).
15. K. Wakabayashi, *Phys. Rev. B* 64, 125428 (**2001**).
16. N. M. R. Peres, A. H. Castro Neto, and F. Guinea, *Phys. Rev. B* 73, 195411 (**2006**).
17. D. Finkenstadt, G. Pennington, and M. J. Mehl, *Phys. Rev. B* 76, 121405 (**2007**).
18. A. Lherbier, B. Biel, Y. Niquet, and S. Roche, *Phys. Rev. Lett.* 100, 036803 (**2008**).
19. C. P. Chang, B. R. Wu, R. B. Chen, and M. F. Lin, *J. Appl. Phys.* 101, 063506 (**2007**).
20. L. Brey and H. A. Fertig, *Phys. Rev. B* 75, 125434 (**2007**).
21. K. Nakada and M. Fujita, *Phys. Rev. B* 54, 24 (**1996**).
22. M. Fujita, K. Wakabayashi, K. Nakada, and K. Kusakabe, *J. Phys. Soc. Jpn.* 65, 1920 (**1996**).
23. Y. C. Huang, C. P. Chang, and M. F. Lin, *Nanotechnol.* 18, 495401 (**2007**).
24. J. E. Müller, *Phys. Rev. Lett.* 68, 385 (**1992**).
25. F. M. Peeters and A. Matulis, *Phys. Rev. B* 48, 15166 (**1993**).
26. I. S. Ibrahim and F. M. Peeters, *Phys. Rev. B* 52, 17321 (**1995**).
27. H. A. Carmona, A. K. Geim, A. Nogaret, P. C. Main, T. J. Foster, and M. Henini, *Phys. Rev. Lett.* 74, 3009 (**1995**).
28. P. D. Ye, D. Weiss, R. R. Gerhardts, M. Seeger, K. V. Klitzing, K. Eberl, and H. Nickel, *Phys. Rev. Lett.* 74, 3013 (**1995**).
29. R. R. Gerhardts, *Phys. Rev. B* 53, 11064 (**1995**).

30. R. R. Gerhardts, *Phys. Rev. B* 53, 11064 (**1995**); A. Nogaret and S. J. Bending, *Phys. Rev. Lett.* 84, 2231 (**2000**).
31. F. M. Peeters and P. Vasilopoulos, *Phys. Rev. B* 47, 1466 (**1993**).
32. C. W. J. Beenakker, *Phys. Rev. Lett.* 62, 2020 (**1989**).
33. A. Matulis and F. M. Peeters, *Phys. Rev. Lett.* 72, 1518 (**1994**).
34. S. Park and H.-S. Sim, *Phys. Rev. B* 77, 075433 (**2008**).
35. J. C. Charlier, J. P. Michenaud, X. Gonze, and J. P. Vigneron, *Phys. Rev. B* 44, 237 (**1991**).
36. H. S. Sim, K. H. Ahn, and K. J. Chang, *Phys. Rev. Lett.* 80, 1501 (**1998**).
37. Y. Kobayashi, K. Fukui, T. Enoki, K. Kusakabe, and Y. Kaburagi, *Phys. Rev. B* 71, 193406 (**2005**).
38. Y. Kobayashi, K. Fukui, and T. Enoki, *Phys. Rev. B* 73, 125415 (**2006**).
39. Y. Niimi, T. Matsui, H. Kambara, K. Tagami, M. Tsukada, and H. Fukuyama, *Phys. Rev. B* 73, 085421 (**2006**).
40. P. Kim, T. W. Odom, J.-L. Huang, and C. M. Lieber, *Phys. Rev. Lett.* 82, 1225 (**1999**).
41. L. C. Venema, J. W. Janssen, M. R. Buitelaar, J. W. G. Wildöer, S. G. Lemay, L. P. Kouwenhoven, and C. Dekker, *Phys. Rev. B* 62, 5238 (**2000**).
42. T. W. Odom, J.-L. Huang, P. Kim, and C. M. Lieber, *J. Phys. Chem. B* 104, 2794 (**2000**).
43. A. Jorio, G. S. Filho, G. Dresselhaus, M. S. Dresselhaus, R. Saito, J. H. Hafner, C. M. Lieber, F. M. Matinaga, M. S. Dantas, and M. A. Pimenta, *Phys. Rev. B* 63, 245416 (**2001**).
44. M. S. Strano, S. K. Doorn, E. H. Haroz, C. Kittrell, R. H. Hauge, and R. E. Smalley, *Nano Lett.* 3, 1091 (**2003**).
45. L. M. Malard, J. Nilsson, D. C. Elias, J. C. Brant, F. Plentz, E. S. Alves, A. H. Castro Neto, and M. A. Pimenta, *Phys. Rev. B* 76, 201401 (**2007**).
46. M. J. O'Connell, S. M. Bachilo, C. B. Huffman, V. C. Moore, M. S. Strano, E. H. Haroz, K. L. Rialon, P. J. Boul, H. W. Noon, C. Kittrell, J. Ma, R. H. Hauge, R. B. Weisman, and R. E. Smalley, *Science* 297, 593 (**2002**).
47. S. M. Bachilo, M. S. Strano, C. Kittrell, R. H. Hauge, R. E. Smalley, and R. B. Weisman, *Science* 298, 2361 (**2002**).
48. J. Lefebvre, Y. Homma, and P. Finnie, *Phys. Rev. Lett.* 90, 217401 (**2003**).
49. S. Lebedkin, F. Hennrich, T. Skipa, and M. M. Kappes, *J. Phys. Chem. B* 107, 1949 (**2003**).
50. N. Malkova, *Phys. Rev. B* 63, 035317 (**2001**).

Received: 16 May 2008. Accepted: 29 July 2008.

RESEARCH ARTICLE